Intelligent Reflecting Surfaces Based Offset Index Modulation for MIMO Systems

Guoying Zhang, *Student Member, IEEE,* Xue-Qin Jiang, *Senior Member, IEEE,* Han Hai, *Member, IEEE,*
Lexi Xu, *Senior Member, IEEE,* Shahid Mumtaz, *Senior Member, IEEE*

Abstract—In this paper, we introduce the concept of offset to the field of intelligent reflecting surfaces-based index modulation (IRS-IM) and propose an IRS-based offset IM (IRS-OIM) scheme. The IRS-OIM scheme not only divides the IRS elements into several blocks but also introduces an offset at the transmitter while reducing the number of IRS controller operations. Furthermore, we develop three offset IRS block selection (OIBS) approaches to adapt to different numbers of activated IRS blocks for IRS-OIM. Compared with IRS-IM, the IRS-OIM increases the reliability of information transmission and ensures a high effective gain for the IRS while increasing the data transmission rate. In addition, the mathematical expression for the average bit error probability (ABEP) of the IRS-OIM scheme is deduced. Comparison between IRS-OIM and their counterparts in terms of complexity is also provided. Monte Carlo simulation results demonstrate the superiority of the proposed IRS-OIM scheme, and show that IRS-OIM achieves more balanced trade-off among complexity and performance than their counterparts.

Index Terms—Intelligent reflecting surface (IRS), offset index modulation (OIM), average bit error probability (ABEP), Multiple-input multiple-output (MIMO).

I. INTRODUCTION

PURSUING the realization of the 6th generation (6G) communication system, researchers delve into pioneering communication technologies [1]–[3]. Multiple-input multiple-output (MIMO) [4] is a key technology for the 6G [5] communication systems. It must be addressed that MIMO systems tend to become progressively more complex as the number of antennas increases. Against this background, index modulation (IM) [6]–[8] systems came into being.

Compared to conventional MIMO systems, IM utilizes the indices of the building blocks, such as transmitting antennas (TAs) [9]–[11], spreading codes [12]–[14] and sub-carriers [15]–[17], and so on [18]–[20], to convey information. Thus,

Xue-Qin Jiang (Corresponding author), Guoying Zhang, and Han Hai are with the College of Information Science and Technology, Donghua University, Shanghai 201620, China (e-mail: xqjiang@dhu.edu.cn, 1209109@mail.dhu.edu.cn, and hhai@dhu.edu.cn, respectively).

Lexi Xu is with the Research Institute, China United Network Communications Corporation, Beijing 100048, China (e-mail: davidlexi@hotmail.com).

Shahid Mumtaz is with Department of Applied Informatics, Silesian University of Technology Akademicka 16 44-100 Gliwice, Poland and also with the Department of Computer Sciences, Nottingham Trent University, NG1 4FQ Nottingham, U.K.(e-mail: dr.shahid.mumtaz@ieee.org)

IM has become increasingly popular owing to being high spectral efficiency (SE) and energy efficiency (EE). Researchers have recently proposed many exciting works in IM [21]–[24]. Notably, spatial modulation (SM) [25] and space shift keying (SSK) [26] are popular IM techniques that convey information by the indices of TAs. In SM and SSK, only a single antenna is used to convey information in each transmission time slot, which means that only a single radio frequency (RF) chain is required in both SM and SSK [27]–[31]. Nevertheless, the maximum switching frequency or minimum switching time between the RF chain and TAs determines the transmission rates of SM and SSK [32].

To alleviate this bottleneck for future broadband wireless communication applications, offset SM (OSM) and offset SSK (OSSK) were developed in [33]. The OSM and OSSK schemes can provide a flexible tradeoff between the switching frequency and the bit error rate (BER) performance by introducing an offset between the connected RF chain and the index of the active antenna. In [34], the OSM scheme was combined with orthogonal frequency division multiplexing (OFDM) using channel state information (CSI) aided precoding at the transmitter, which simplifies the structure and reduces RF chains. The peak-to-average power ratio (PAPR) reduction techniques along with the performance evaluation of the OSM-OFDM scheme were studied in [35]. In [36], the OSM-MIMO and OSSK-MIMO schemes were extended to adapt multiple-input single-output (MISO) systems, which introduce multiple receiver antennas (RAs). TA selection was integrated with the OSM scheme in [37], which is developed toward a flexible tradeoff between scheme performance and computational complexity.

Intelligent reflective surfaces (IRS) consist of a large number of passively reconfigurable IRS elements in a flat surface, which can improve SE and EE [38]. Thus, the development of IRS-based communication schemes has been of increasing interest [39]–[41]. The authors in [42] pointed out how SM can evolve to IRS-based modulation while maintaining the single RF chain. The generalized/quadrature SM concept was first adopted in [43] and [44] for designing IRS-IM schemes, which can be used as a powerful strategy for symbiotic communications. The reconfigurable intelligent surface (RIS) grouping-based IM (RGB-IM) was designed in [45], which improves SE by using the activation of the IRS group indices to convey information. However, the RGB-IM scheme reduces the effective gain of the IRS compared to IRS-based IM, which utilizes all IRS elements.

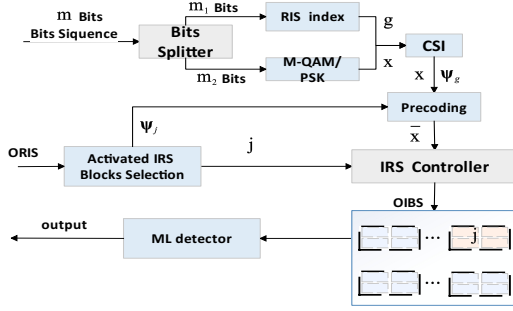Motivated by previous work on RGB-IM and OSM, the

Fig. 1. System model of the IRS-OIM scheme.

IRS-based offset IM (IRS-OIM) scheme is proposed in this paper to improve the reliability of information transmission and the effective gain of the IRS. Specifically, we divide the IRS elements into several blocks and introduce an offset between the antennas and IRS blocks. In addition, three offset IRS block selection (OIBS) approaches, namely static OIBS (S-OIBS), dynamic optimal OIBS (DO-OIBS), and dynamic multi-activation OIBS (DMA-OIBS), are provided. Specifically, S-OIBS has a fixed offset IRS block. The number of IRS controller operations can be reduced when the offset IRS block is determined. DO-OIBS and DMA-OIBS select the offset IRS block based on the channel gain. The former selects the optimal IRS block offset, such that the number of IRS controller operations is slightly higher than that of S-OIBS, while BER performance outperforms that of S-OIBS. The latter selects multiple offset IRS blocks, so the complexity is higher than that of S-OIBS and DO-OIBS, while the IRS energy gain and BER performance are further improved. These three approaches result in different performance gains on limiting different numbers of controller operations and activated IRS blocks. Also, the average bit error probability (ABEP) is derived for evaluating the performance of the IRS-OIM systems. Furthermore, the comparison of the IRS-OIM, and RGB-IM schemes is provided. The simulation and theoretical analysis show that the proposed IRS-OIM scheme has an excellent improvement in terms of BER performance. The remainder of this paper is organized as follows. Section II elaborates on the system model of the proposed IRS-OIM scheme. In Section III, the details of three OIBS approaches are proposed. The ABEP upper bound of the IRS-OIM scheme is derived in Section IV. A complexity comparison is presented in Section V. Simulation results are given in Section VI. Finally, conclusions are offered in Section VII.

Notations: Bold upper case letters denote matrices, and bold lower case boldface letters represent vectors, and lower case non-boldface letters stand for scalars. $(\cdot)^T$ stands for transpose operation. $\mathbb{C}^{a \times b}$ denotes the space of $a \times b$ complex matrices. $\odot$ denotes the Hadamard product. $\mathbf{0}_{n,m}$ denotes an all-zero matrix of size $n \times m$. $\binom{\cdot}{\cdot}$ denotes the binomial coefficient. $|\cdot|$ denotes the absolute value of a complex scalar. $\mathrm{diag}(a)$ denotes a diagonal matrix with the diagonal elements a. $P(\cdot)$ denotes the probability of an event. $\lfloor \cdot \rfloor$ denotes the floor function that

maps a real number to its integer part. $|\cdot|$ denotes the absolute value.

II. SYSTEM MODEL

As shown in Fig.1, we consider the IRS-OIM system, which comprises N_t TAs, N_r receiving antennas (RAs), an IRS controller, and N IRS elements.

In IRS-OIM, the IRS is divided into G blocks, each consisting of S IRS elements such that $N = G \times S$. The channel from the TAs to the IRS is denoted by $\mathbf{H} \in \mathbb{C}^{N \times N_t} \triangleq [\mathbf{H}_1, \cdots, \mathbf{H}_g, \cdots, \mathbf{H}_G]^T$, while the channel from the IRS to the RAs is represented by $\mathbf{D} \in \mathbb{C}^{N_r \times N} \triangleq [\mathbf{D}_1, \cdots, \mathbf{D}_g, \cdots, \mathbf{D}_G]$, where $\mathbf{H}_g \in \mathbb{C}^{S \times N_t}$ and $\mathbf{D}_g \in \mathbb{C}^{N_r \times S}$ denote the corresponding channels associated with the IRS block g. Let $\mathbf{\Phi} \in \mathbb{C}^{N \times N} \triangleq [\mathbf{\Phi}_1, \cdots, \mathbf{\Phi}_g, \cdots, \mathbf{\Phi}_G]$ denotes the IRS phase shifter, where $\mathbf{\Phi}_g \in \mathbb{C}^{S \times S}$. Then the cascaded channel for the TAs→IRS block g→RAs is denoted by

$$\mathbf{\Psi}_g = \mathbf{D}_g \mathbf{\Phi}_g \mathbf{H}_g, \qquad (1)$$

where $\mathbf{D}_g(r,s) = d_{r,g,s}$, $\mathbf{\Phi}_g(s,s) = \phi_{s,g,s}$, $\mathbf{H}_g(s,t) = h_{s,g,t}$, $r \in (1, N_r)$, $s \in (1, S)$, $t \in (1, N_t)$, and $\mathbf{\Psi}_g(r,t) = \sum_{s=1}^{S} d_{r,g,s} \phi_{s,g,s} h_{s,g,t}$ denotes the cascaded channel for the TA t→IRS block g→RA r.

In Fig. 1, $\mathbf{m}$ with dimensions $m \times 1$ is a vector of information bits to be transmitted during T_c symbol period, which is divided into two parts and the data rate of the IRS-OIM is

$$\gamma = m_1 + m_2 = \log_2 G + \log_2 M. \qquad (2)$$

The first m_1 bits are used to select the index g of IRS blocks and the second m_2 bits determine the modulated symbol s, which is modulated by M-QAM/PSK. Consequently, the index g of IRS blocks combined with the modulated symbol s make up the transmit symbol $x_{g,t}$, which is transmitted by the TA t and reflected by the IRS block g. Then, the transmit vector can be expressed as

$$\mathbf{x} = [x_{g,1}, \cdots, x_{g,t}, \cdots, x_{g,N_t}]^T, g \in \{1, \ldots, G\}. \quad (3)$$

$\mathbf{x}$ will be further offset to a predetermined activation IRS block j. This means that the IRS block g will be switched to the IRS block j via the IRS controller, and $\mathbf{x}$ is offset to $\bar{\mathbf{x}}$, where

$$\bar{\mathbf{x}} = [x_{j,1}, \cdots, x_{j,t}, \cdots, x_{j,N_t}]^T, j \in \{1, \ldots, G\}. \quad (4)$$

Remark: To make a better trade-off between information reliability and utilization of the IRS, we let $N_t = N_r$ and give three approaches to determine the index of activated IRS block j, which will be introduced in the next section. ∎

Let ρ denotes the transmit power, $\mathbf{\Psi} \in \mathbb{C}^{N_r \times N_t} \triangleq \mathbf{D}\mathbf{\Phi}\mathbf{H}$ denotes the cascaded channel for the TAs→IRS blocks→RAs, and $\mathbf{N}$ denotes an additive white Gaussian noise (AWGN). The elements of $\mathbf{\Psi}$ and $\mathbf{N}$ have independent and identically distributed (iid) entries according to $\mathcal{CN}(0,1)$. The received signal can be expressed as (5), shown at the bottom of this page.
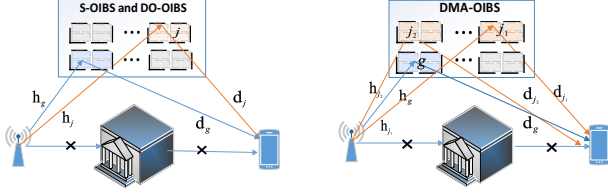
(a) S-OIBS and DO-OIBS.   (b) DMA-OIBS.

Fig. 2.   Working principles of S-OIBS, DO-OIBS and DMA-OIBS.

At the receiver, the objective function of the detector adopting ML criterion for IRS-OSM can be formulated as

$$[\hat{s}, \hat{g}] = \arg \min_{s \in \mathbb{M}, g \in \chi} \left| \mathbf{Y} - \sqrt{\rho} \mathbf{\Psi}_j \bar{\mathbf{x}} \right|, \tag{6}$$

where $\mathbb{M}$ denotes the constellation set, $\chi = \{1, \ldots, g, \ldots, G\}$.

III. OFFSET APPROACH

This section introduces three OIBS methods, i.e.,S-OIBS, DO-OIBS, and DMA-OIBS, for selecting the index j of the activated IRS block. S-OIBS allows the IRS controller to switch on only a fixed IRS block, which avoids frequent controller operation. DO-OIBS allows the IRS controller to switch on a different IRS block according to the channel gain, which enables better performance than RGB-IM. DMA-OIBS allows the IRS controller to switch on more than one IRS block according to the channel gain, which improves the effective gain of the IRS.

A. S-OIBS

In S-OIBS, $\mathbf{x}$ is switched from $\mathbf{\Psi}_g$ to $\mathbf{\Psi}_j$, where g is the spatially modulated index of IRS blocks, and j is the arbitrarily fixed index of IRS blocks. The working principle of the S-OIBS is shown in Fig. 2 (a).

When j is fixed, for the given (3) and cascaded channel $\mathbf{\Psi}_g$, $\mathbf{x}$ will be precoded as [33]

$$\bar{\mathbf{x}} = \mathbf{\Psi}_j^{-1} \mathbf{\Psi}_g \boldsymbol{\beta}^j \mathbf{x}, \tag{7}$$

where $\boldsymbol{\beta}^j = \left| \mathbf{\Psi}_g^{-1} \mathbf{\Psi}_j \right|$ is the normalized transmit power factor. Then, the received signal can be further derived as

$$\begin{aligned} \mathbf{Y} &= \sqrt{\rho} \mathbf{\Psi}_j \bar{\mathbf{x}} + \mathbf{N} = \sqrt{\rho} \mathbf{\Psi}_j \mathbf{\Psi}_j^{-1} \mathbf{\Psi}_g \boldsymbol{\beta}^j \mathbf{x} + \mathbf{N} \\ &= \sqrt{\rho} \mathbf{\Psi}_g \boldsymbol{\beta}^j \mathbf{x} + \mathbf{N}. \end{aligned} \tag{8}$$

Finally, 6 can be rewritten as

$$[\hat{s}, \hat{g}] = \arg \min_{s \in \mathbb{M}, g \in \chi} \left| \mathbf{Y} - \sqrt{\rho} \mathbf{\Psi}_g \boldsymbol{\beta}^j \mathbf{x} \right|. \tag{9}$$

In this case, the activated IRS block j is arbitrarily fixed. This approach avoids the operation of the IRS controller. When the parameter settings are the same as RGB-IM, a performance comparable to that of RGB-IM is obtained.

B. DO-OIBS

The working principle of the DO-OIBS is also shown in Fig. 2 (a). In DO-OIBS, $\mathbf{x}$ is also switched from $\mathbf{\Psi}_g$ to $\mathbf{\Psi}_j$. Distinguished from S-OIBS, j is determined by maximizing the channel gain.

Specifically, j is selected from $\bar{\chi} = \{1, \ldots, g, \ldots, p\}$, $1 \leq p \leq G$, which can be expressed as

$$j = \arg \max_{g \in \bar{\chi}} |\delta_g|, \quad \delta_g = (\det(\mathbf{\Psi}_g \mathbf{\Psi}_g^T))^{1/2}. \tag{10}$$

When j is fixed, $\mathbf{x}$ will be precoded as (7) and $\mathbf{Y}$ can be expressed as (8).

In this case, the activated IRS block j depends on the channel gain. The DO-OIBS has a similar number of IRS controller operations compared to the RGB-IM. Nevertheless, the BER performance of DO-OIBS will be better than RGB-IM. Compared to S-OIBS, DO-OIBS activates variable IRS blocks, increasing controller operation and improving BER performance. Furthermore, the performance of the IRS-OIM with DO-OIBS can be significantly improved as p increases.

C. DMA-OIBS

In DMA-OIBS, $\mathbf{x}$ is switched from $\mathbf{\Psi}_g$ to $\mathbf{\Psi}_{j_1}, \ldots, \mathbf{\Psi}_{j_i}$, $\ldots, \mathbf{\Psi}_{j_n}$, where j_i is the index of the activated IRS block. In this case, we use the channel gain to select the best activated index set $\mathbf{J}$ of the IRS block.

To generate the set $\mathbf{J}$, we first arrange $|\delta_g|$ in descending order and denote as

$$\bar{\mathbf{J}} = \left\{ \left| \bar{\delta}_1 \right|, \cdots, \left| \bar{\delta}_g \right|, \cdots, \left| \bar{\delta}_G \right| \right\}. \tag{11}$$

Then, the indices corresponding to the elements in $\bar{\mathbf{J}}$ before they are arranged in descending order and are determined to form the activated index set $\hat{\mathbf{J}}$ of the IRS block, where

$$\hat{\mathbf{J}} = \{j_1, \ldots, j_n, \ldots, j_G\}, \text{ and } j_n \in \{1, \ldots, G\}. \tag{12}$$

Finally, the first n elements in $\hat{\mathbf{J}}$, i.e. n activated IRS blocks, are selected to generate $\mathbf{J}$, where $\mathbf{J} = \{j_1, j_2, \ldots, j_n\}$. Fig. 2 (b) further demonstrates the working principle of DMA-OIBS.

$$\begin{aligned} \mathbf{Y} = \sqrt{\rho} \mathbf{\Psi} \bar{\mathbf{x}} + \mathbf{N} &= \sqrt{\rho} \begin{bmatrix} \mathbf{D}_1 & \cdots & \mathbf{D}_j & \cdots & \mathbf{D}_G \end{bmatrix} \begin{bmatrix} \mathbf{0}_1 & & & & \\ & \ddots & & & \\ & & \mathbf{\Phi}_j & & \\ & & & \ddots & \\ & & & & \mathbf{0}_G \end{bmatrix} \begin{bmatrix} \mathbf{H}_1 \\ \vdots \\ \mathbf{H}_j \\ \vdots \\ \mathbf{H}_G \end{bmatrix} \bar{\mathbf{x}} + \mathbf{N} \\ &= \sqrt{\rho} \mathbf{D}_j \mathbf{\Phi}_j \mathbf{H}_j \bar{\mathbf{x}} + \mathbf{N} = \sqrt{\rho} \mathbf{\Psi}_j \bar{\mathbf{x}} + \mathbf{N}. \end{aligned} \tag{5}$$

When $\mathbf{J}$ is fixed, $\mathbf{x}$ will be precoded as

$$\bar{\mathbf{x}} = \mathbf{\Psi}_{j_1}^{-1}\mathbf{\Psi}_g\boldsymbol{\beta}^{j_1}\mathbf{x} + \cdots + \mathbf{\Psi}_{j_n}^{-1}\mathbf{\Psi}_g\boldsymbol{\beta}^{j_n}\mathbf{x}, \qquad (13)$$

and the received signal $\mathbf{Y}$ can be expressed as

$$\mathbf{Y} = \sqrt{\rho}\mathbf{\Psi}_g\boldsymbol{\beta}^{j_1}\mathbf{x} + \cdots + \mathbf{\Psi}_g\boldsymbol{\beta}^{j_n}\mathbf{x} + \mathbf{N}. \qquad (14)$$

For instance, we consider DMA-OIBS with $G = 4$ and $n = 2$. The set $\bar{\mathbf{J}}$ and $\hat{\mathbf{J}}$ can be denoted as $\bar{\mathbf{J}} = \{|\bar{\delta}_2|, |\bar{\delta}_3|, |\bar{\delta}_1|, |\bar{\delta}_4|\}$ and $\hat{\mathbf{J}} = \{2, 3, 1, 4\}$, respectively. Assuming the indices of $|\bar{\delta}_1|$ and $|\bar{\delta}_2|$ before descending order are 2 and 3, respectively. Then, the best activated index set $\mathbf{J}$ can be denoted as $\mathbf{J} = \{j_1, j_2\} = \{2, 3\}$ and $\mathbf{x}$ will be precoded as $\bar{\mathbf{x}} = \mathbf{\Psi}_2^{-1}\mathbf{\Psi}_g\boldsymbol{\beta}^2\mathbf{x} + \cdots + \mathbf{\Psi}_3^{-1}\mathbf{\Psi}_g\boldsymbol{\beta}^3\mathbf{x}$.

Finally, the ML detection criterion can be rewritten as

$$[\hat{s}, \hat{g}] = \arg\min_{s\in\mathbb{M}, g\in\boldsymbol{\chi}}\left|\mathbf{Y} - \sqrt{\rho}\left(\mathbf{\Psi}_g\boldsymbol{\beta}^{j_1}\mathbf{x} + \cdots + \mathbf{\Psi}_g\boldsymbol{\beta}^{j_n}\mathbf{x}\right)\right|. \qquad (15)$$

In this case, the activated IRS block j depends on the channel gain. Compared to the RGB-IM, it opens additional IRS blocks, and the energy gain of the IRS is further increased. Compared to S-OIBS and DO-OIBS, the number of activated IRS blocks n increases in DMA-OIBS, leading to more controller operations while improving the BER performance. As mentioned above, DMA-OIBS can achieve a dynamic balance between BER performance and the number of controller operations.

IV. RERFORMANCE ANALYSIS

By the asymptotically union bound [46], the ABEP is upper bounded by

$$\mathbb{P}_C \leq \frac{1}{\gamma 2^\gamma}\sum_{i=1}^{\gamma}\sum_{j=1}^{\gamma}e_{i,j}P(\mathbf{x}\rightarrow\hat{\mathbf{x}}), \qquad (16)$$

where $e_{i,j}$ represents the number of error bits in determining $\hat{\mathbf{x}}$ given that $\mathbf{x}$ is transmitted, $P(\mathbf{x}\rightarrow\hat{\mathbf{x}})$ is the pairwise error probability (PEP).

According to [33], The conditional PEP is calculated as

$$P(\mathbf{x}\rightarrow\hat{\mathbf{x}}|\mathbf{\Psi}) \leq Q\left(\sqrt{\frac{\rho\|\boldsymbol{\beta}\|^2\|\mathbf{\Psi}(\mathbf{x}-\hat{\mathbf{x}})\|^2}{4}}\right), \qquad (17)$$

where $Q(x) = \frac{1}{\pi}\int_0^{\frac{\pi}{2}}e^{-\frac{x^2}{2\sin^2\theta}}d\theta$ is the Gaussian Q-function. In S-OIBS and DO-OIBS, $\|\boldsymbol{\beta}\|^2 = \|\boldsymbol{\beta}^j\|^2$, while in DMA-OIBS, $\|\boldsymbol{\beta}\|^2 = \|[\boldsymbol{\beta}^{j_1}, \cdots, \boldsymbol{\beta}^{j_n}]\|^2$. We define $\beta = \|\boldsymbol{\beta}\|^2$ to simplify the analysis. Then (17) can be rewritten as

$$P(\mathbf{x}\rightarrow\hat{\mathbf{x}}|\mathbf{\Psi}) = Q\left(\sqrt{\frac{\rho\beta^2\|\mathbf{\Psi}(\mathbf{x}-\hat{\mathbf{x}})\|^2}{4}}\right). \qquad (18)$$

Denoting $\eta = \frac{\rho\beta^2}{4}\|\mathbf{\Psi}(\mathbf{x}-\hat{\mathbf{x}})\|^2$, the PEP after taking the expectation of $P(\mathbf{x}\rightarrow\hat{\mathbf{x}}|\mathbf{\Psi})$ is expressed as follows

$$P(\mathbf{x}\rightarrow\hat{\mathbf{x}}) = \frac{1}{\pi}\int_0^{\frac{\pi}{2}}\int_{-\infty}^{+\infty}e^{-\frac{\eta}{2\sin^2\theta}}P_\eta(\eta)d\eta d\theta$$
$$= \frac{1}{\pi}\int_0^{\frac{\pi}{2}}M_\eta\left(-\frac{\rho\beta^2}{8\sin^2\theta}\right)d\theta. \qquad (19)$$

where M_η and P_η are the moment generating function (MGF) and the probability density function of η, respectively. To simplify the analysis, we denote

$$\mathbf{V}_{i,j} = (\mathbf{x}-\hat{\mathbf{x}})(\mathbf{x}-\hat{\mathbf{x}})^H = \mathbf{U}\mathbf{\Lambda}_{i,j}\mathbf{U}^H, \qquad (20)$$

where $\mathbf{V}_{i,j}$ is a nonnegative definite Hermitian matrix with rank $r_{i,j}$, $\mathbf{U}$ is a unitary matrix, $\mathbf{\Lambda}_{i,j} = \text{diag}(\lambda_{i,j,1}, \ldots, \lambda_{i,j,N_t})$ is the eigenvalue matrix of $\mathbf{V}_{i,j}$. Denote $\hat{\mathbf{\Psi}} = \mathbf{\Psi}\mathbf{U}$, η can be further derived as

$$\eta = \frac{\rho\beta^2}{4}Tr\left[\mathbf{\Psi}\mathbf{V}_{i,j}\mathbf{\Psi}^H\right] = \frac{\rho\beta^2}{4}Tr\left[\hat{\mathbf{\Psi}}\mathbf{\Lambda}_{i,j}\hat{\mathbf{\Psi}}^H\right]$$
$$= \frac{\rho\beta^2}{4}\sum_{n=1}^{N_r}\sum_{m=1}^{N_t}\lambda_{i,j,m}|\hat{\psi}_{n,m}|^2 = \frac{\rho\beta^2}{4}\sum_{n=1}^{N_r}\sum_{m=1}^{r_{i,j}}\lambda_{i,j,m}|\hat{\psi}_{n,m}|^2, \qquad (21)$$

where $\hat{\psi}_{n,m}$ is the element in the n-th row and m-th column in $\hat{\mathbf{\Psi}}$. Let $\eta' = \sum_m^{N_t}\lambda_{i,j,m}|\hat{\psi}_{n,m}|^2$, the $M_{\eta'}(q)$ can be derived as

$$M_{\eta'}(q) = \prod_{n=1}^{N_r}\prod_{m=1}^{r_{i,j}}M_{\eta_n}(q)$$
$$= \prod_{m=1}^{r_{i,j}}(1 - \lambda_{i,j,m}q)^{-N_r}, \qquad (22)$$

where $\eta_n = \lambda_{i,j,m}|\hat{\psi}_{n,m}|^2$. According to the property of MGF, the MGF of η can be obtained as

$$M_\eta(q) = \prod_{m=1}^{r_{i,j}}(1 + \frac{\rho\beta^2\lambda_{i,j,m}}{8\sin^2\theta})^{-N_r}$$
$$\leq \prod_{m=1}^{r_{i,j}}(1 + \frac{\rho\beta^2\lambda_{i,j,m}}{8})^{-N_r}. \qquad (23)$$

Thus, (19) can be further derived as

$$Pr(\mathbf{x}\rightarrow\hat{\mathbf{x}}) \leq \frac{1}{2}\prod_{m=1}^{r_{i,j}}\left(1 + \frac{\rho\beta^2\lambda_{i,j,m}}{8}\right)^{-N_r}. \qquad (24)$$

By substituting (24) into (16), the ABEP upper bound can be obtained as

$$\mathbb{P}_C \leq \frac{1}{\gamma 2^{\gamma+1}}\sum_{i=1}^{\gamma}\sum_{j=1}^{\gamma}e_{i,j}\prod_{m=1}^{r_{i,j}}\left(\frac{8}{8 + \rho\beta^2\lambda_{i,j,m}}\right)^{N_r}. \qquad (25)$$

V. COMPLEXITY ANALYSIS

In this section, we present the computational complexity in terms of the number of floating point operations (FLOPs) for complex multiplication [47]. Table I shows the complexity of IRS-OIM with S-OIBS, DO-OIBS and DMA-OIBS, respectively, and RGB-IM, where $\mathcal{O}_{RGB-IM}$ is the complexity of RGB-IM.

As seen from Table I, the IRS-OIM requires more FLOPs than the RGB-IM due to the offset. Fig. 3 shows the detailed complexity of IRS-OIM with S-OIBS, DO-OIBS, and DMA-OIBS, respectively, and RGB-IM in the case of $(N_t, N_r, M, N, G) = (1, 1, 16, 128, 8)$. Specifically, the complexity of IRS-OIM with DO-OIBS are presented in Fig. 3(a) with $p = 1$ and $p = 2$, the complexity of IRS-OIM with DMA-OIBS are presented with $n = 1$ and $n = 2$. It can be seen from

TABLE I
COMPLEXITY OF IRS-OIM WITH S-OIBS, DO-OIBS, AND DMA-OIBS,
RESPECTIVELY, AND RGB-IM.

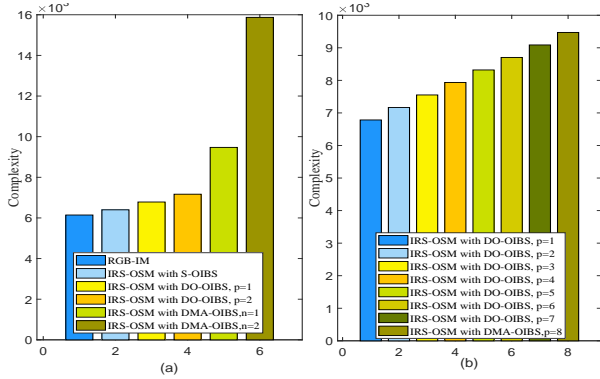| Scheme	Complexity
RGB-IM	$GM(3N_rN_tS)$
IRS-OIM with S-OIBS	$8S + \mathcal{O}_{RGB-IM}$
IRS-OIM with DO-OIBS	$8S + 12N_rN_tSp + \mathcal{O}_{RGB-IM}$
IRS-OIM with DMA-OIBS	$8Sn + 12N_rN_tN + n\mathcal{O}_{RGB-IM}$

Fig. 3. Complexity of IRS-OIM with S-OIBS, DO-OIBS, and DMA-OIBS, respectively, and RGB-IM, IRS-SM, and IRS-SSK.
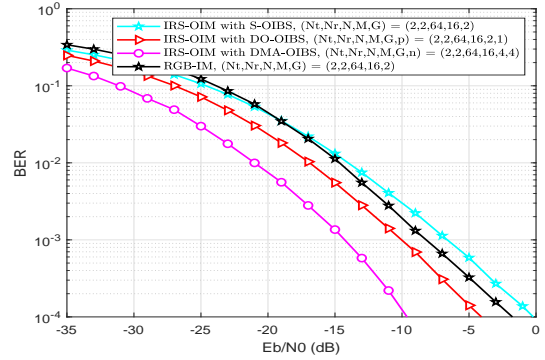

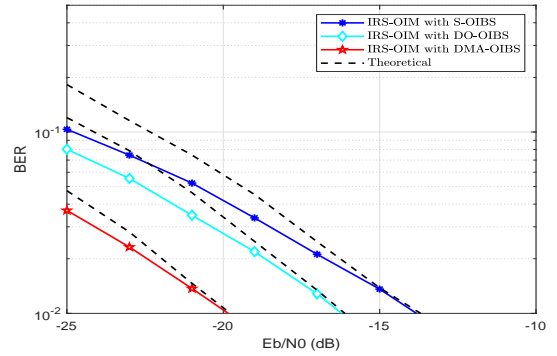Fig. 4. BER performance comparison of IRS-OIM with S-OIBS, DO-OIBS, and DMA-OIBS respectively, and RGB-IM.

Fig. 5. Comparison of theoretical and simulation results of IRS-OIM with S-OIBS, DO-OIBS, and DMA-OIBS respectively.

Fig. 3(a) that the IRS-OIM with S-OIBS exhibits the lowest complexity. The complexity of DO-OIBS is comparable to IRS-OIM with S-OIBS when $p = 1$. In contrast, IRS-OIM with DMA-OIBS indicates the most considerable computation cost. This is because g is only offset to j in S-OIBS and DO-OIBS, while g is offset to several n in DAM-OIBS. In Fig. 3(b), the complexity of IRS-OIM with DO-OIBS are presented with $p = 1, 2, 3, 4, 5, 6, 7, 8$. It can be seen from Fig. 3(b) that the complexity grows linearly with p.

In fact, IRS-OIM provides additional BER performance enhancements at the cost of a modest increase in computational complexity compared to RGB-IM. Specifically, the complexity of IRS-OIM with DO-OIBS increases as p increases, while the BER performance is significantly improved. In the forthcoming BER comparison in the next section, we will show that IRS-OIM exhibits a significant BER performance advantage over RGB-IM.

VI. SIMULATION RESULTS

In this section, the Monte Carlo simulations evaluate the BER performance of the proposed IRS-OIM scheme over Rayleigh fading channels.

Fig. 4 shows the BER performance of IRS-OIM with S-OIBS, DO-OIBS, and DMA-OIBS, respectively, and RGB-IM. The BER performance curves of IRS-OIM and RGB-IM are presented with $(N_t, N_r, N, M, G) = (2, 2, 64, 16, 2)$. In IRS-OIM with S-OIBS, activated IRS block indexes are permanently fixed to the same IRS block. In this case, IRS-OIM achieves comparable performance to RGB-IM. In IRS-OIM with DO-OIBS, the index of activated IRS block changes depending on the channel gain. In this case, IRS-OIM with DO-OIBS provides approximately 2.5dB SNR gain more than RGB-IM at BER $= 10^{-4}$. In IRS-OIM with DMA-OIBS, the indexes of the activated multiple IRS blocks change depending on the channel gain. In this case, the performance gain of IRS-OIM with DMA-OIBS is remarkable compared to RGB-IM. Specifically, IRS-OIM with DMA-OIBS provides approximately 7dB SNR gain than that of RGB-IM at BER $= 10^{-4}$.

The IRS-OIM in theoretical and simulation results are displayed in Fig. 5. The IRS-OIM with S-OIBS, DO-OIBS and DMA-OIBS are considered with $(N_t, N_r, N, M, G) = (2, 2, 256, 4, 8)$, $(N_t, N_r, N, M, G) = (2, 2, 128, 8, 8)$, $(N_t, N_r, N, M, G) = (2, 2, 128, 8, 4)$, respectively, in Fig. 5. Note that the tight bounds on the BER of the IRS-OIM match the simulation results.

In Fig. 6, we present the BER performance comparison of IRS-OIM with S-OIBS, DO-OIBS, and DMA-OIBS schemes for $\sigma_e^2 = 0.01/0.05$. When the channel estimation error is considered, the channel matrix is estimated at the receiver as $\hat{\boldsymbol{\Psi}} = \boldsymbol{\Psi} + \boldsymbol{\Psi}_e$, where φ_e represents the vector of channel estimation errors with the distribution $\mathcal{CN}(0, \sigma_e^2\mathbf{I})$, and it is independent of $\boldsymbol{\Psi}$. $\hat{\boldsymbol{\Psi}}$ is dependent on $\boldsymbol{\Psi}$ and follows the
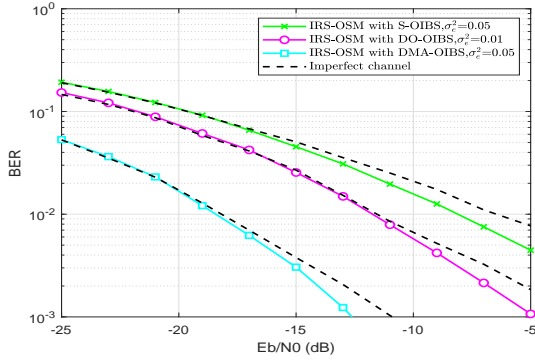
Fig. 6. Comparison of perfect channel information and imperfect channel information of IRS-OIM with S-OIBS, DO-OIBS, and DMA-OIBS respectively.

distribution $\mathcal{CN}(0, (1 + \sigma_e^2)\mathbf{I})$. The conclusion obtained in Fig. 6 is approximately similar to the case of perfect channel estimation.

Fig. 7 depicts the BER curves of the IRS-OIM with S-OIBS and DO-OIBS, respectively, and RGB-IM with different p values. When $(N_t, N_r, N, M, G) = (1, 1, 128, 16, 8)$, DO-OIBS with $p = 8$ provide 3dB SNR gains at a BER of 10^{-1} against $n = 4$, while DO-OIBS with $p = 4$ provide 4dB SNR gains at a BER of 10^{-1} against $n = 2$. When $p > 1$, the IRS-OIM with DO-OIBS achieves an impressive performance gain over RGB-IM. Therefore, it is possible to effectively increase the performance gain by carefully selecting p in DO-OIBS.

Fig. 8 depicts the comparison of IRS-OIM with DMA-OIBS with different n. When $(N_t, N_r, N, M, G) = (2, 2, 128, 16, 4)$, DMA-OIBS with $n = 4$ provide 7dB SNR gains at a BER of 10^{-3} against $n = 2$. As the number of activated IRS block n increases, the BER performance of IRS-OIM with DMA-OIBS is improved, which may lead to a tradeoff between the BER performance and effective gain.

Fig. 9 depicts the BER curves of the IRS-OIM with S-OIBS and DO-OIBS, respectively, under $P = G$. The RGB-IM is considered with $(Nt, Nr, N, M, G) = (2, 2, 64, 16, 2)$ and $(Nt, Nr, N, M, G) = (2, 2, 64, 16, 4)$ respectively. The IRS-OIM with DO-OIBS is considered with $(Nt, Nr, N, M, G, P) = (2, 2, 64, 16, 2, 2)$ and $(Nt, Nr, N, M, G, P) = (2, 2, 64, 16, 4, 4)$. The performance of IRS-OSM with DO-OIBS will be better than RGB-IM when $P = G$. This is because IRS-OIM with DO-OIBS selects the optimal offset IRS block via the channel gain.

VII. CONCLUSION

In this paper, we have proposed a scheme named IRS-OIM. In IRS-OIM, dividing the IRS elements into blocks provides higher data rates. As expected, the introduction of an offset between the TA/RA as well as the index of the IRS block increases the reliability of the information transmission and ensures a high effective gain of the IRS. Specifically, three OIBS approaches, named static OIBS, optimal dynamic OIBS, and multi-activation dynamic OIBS, have been investigated. Furthermore, simulations also derived and verified the ABER upper bound of the proposed IRS-OIM. Simulation results
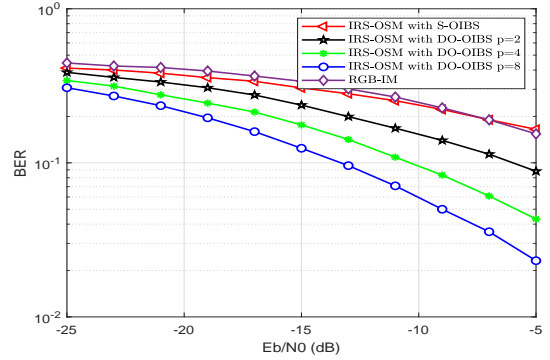

Fig. 7. BER performance comparison of RGB-IM, IRS-OIM with S-OIBS and DO-OIBS with different p, $N = 128$, $M = 16$, $G = 8$.
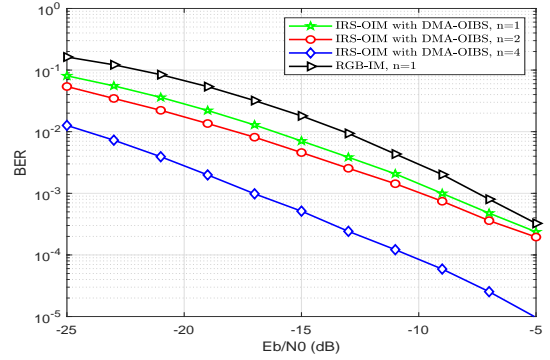

Fig. 8. BER performance comparison of IRS-OIM with DO-OIBS and DMA-OIBS with different n, $N = 128$, $M = 16$, $G = 4$.
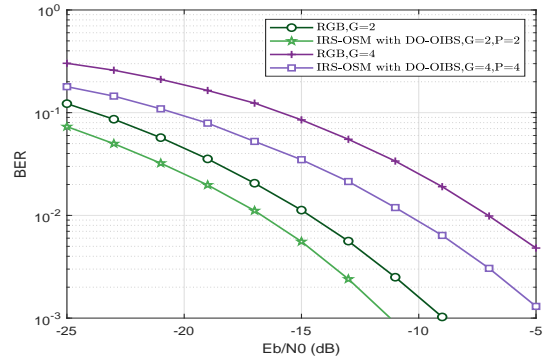

Fig. 9. BER performance comparison of IRS-OIM with DO-OIBS and DMA-OIBS in the case of $P = G$.

have shown that the performance gains can be effectively improved by carefully selecting p in the IRS-OIBS.

REFERENCES

[1] P. H. Pathak, X. Feng, P. Hu and P. Mohapatra, "Visible light communication, networking, and sensing: a survey, potential and challenges," *IEEE Commun. Surv. Tutor.*, vol. 17, no. 4, pp. 2047-2077, Fourthquarter 2015.

[2] D. Wan, M. Wen, F. Ji, H. Yu and F. Chen, "Non-orthogonal multiple access for cooperative communications: challenges, opportunities, and trends," *IEEE Wirel. Commun.*, vol. 25, no. 2, pp. 109-117, Apr. 2018.

[3] Z. Zhang, Y. Xiao, Z. Ma, M. Xiao, Z. Ding, X. Lei, G. K. Karagiannidis, and P. Fan, "6g Wireless networks: vision, requirements, architecture, and key technologies," *IEEE Veh. Technol. Mag.*, vol. 14, no. 3, pp. 28-41, Jul. 2019.

[4] J. Mietzner, R. Schober, L. Lampe, W. Gerstacker, and P. Hoeher, "Multiple-antenna yechniques for wireless communications-a comprehensive literature survey," *IEEE Commun. Surveys Tuts.*, vol. 11, no. 2, pp. 87-105, Apr.-Jun. 2009.

[5] D. Soldani, and A. Manzalini, "6G: The next frontier," *IEEE Veh. Technol. Mag.*, vol. 14, no. 3, pp. 42-50, Sep. 2019.

[6] E. Basar, "Index modulation techniques for 5G wireless networks," *IEEE Commun. Mag.*, vol. 54, no. 7, pp. 168-175, Jul. 2016.

[7] E. Basar, M. Wen, R. Mesleh, M. Di Renzo, Y. Xiao and H. Haas, "Index modulation techniques for next-generation wireless networks," *IEEE Access*, vol. 5, pp. 16693-16746, 2017.

[8] T. Mao, Q. Wang, Z. Wang and S. Chen, "Novel index modulation techniques: a survey," *IEEE Commun. Surv. Tutor.*, vol. 21, no. 1, pp. 315-348, Firstquarter 2019.

[9] R. Y. Mesleh, H. Haas, S. Sinanovic, C. W. Ahn and S. Yun, "Spatial modulation," *IEEE Trans. Veh. Technol.*, vol. 57, no. 4, pp. 2228-2241, July 2008.

[10] M. Di Renzo, H. Haas, A. Ghrayeb, S. Sugiura and L. Hanzo, "Spatial modulation for generalized MIMO: challenges, opportunities, and implementation," *Proc IEEE Inst Electr Electron Eng*, vol. 102, no. 1, pp. 56-103, Jan. 2014.

[11] M. Wen, B. Zheng, K. J. Kim, M. Di Renzo, T. A. Tsiftsis, K. - C. Chen, N. Al-Dhahir, "A survey on spatialmodulation in emerging wireless systems: research progresses and applications," *IEEE J. Sel. Areas Commun.*, vol. 37, no. 9, pp. 1949-1972, Sept. 2019.

[12] G. Kaddoum, M. F. A. Ahmed and Y. Nijsure, "Code index modulation: a high data rate and energy efficient communication system," *IEEE Commun. Lett.*, vol. 19, no. 2, pp. 175-178, Feb. 2015.

[13] G. Kaddoum, Y. Nijsure, and H. Tran, "Generalized code Index modulation technique for high-data-rate communication systems," *IEEE Trans. Veh. Technol.*, vol. 65, no. 9, pp. 7000-7009, Sept. 2016.

[14] W. Xu, Y. Tan, F. C. M. Lau and G. Kolumban, "Design and optimization of differential chaos shift keying scheme with code index modulation," *IEEE Trans. Commun.*, vol. 66, no. 5, pp. 1970-1980, May 2018.

[15] R. Abu-alhiga and H. Haas, "Subcarrier-index modulation OFDM," in *Proc. IEEE 20th Int. Sym. Personal, Indoor, Mobile Radio Commun.*, 2009, pp. 177-181.

[16] D. Tsonev, S. Sinanovic and H. Haas, "Enhanced subcarrier index modulation (SIM) OFDM, in *2011 Proc. IEEE GLOBECOM Workshops*, pp. 728-732, 2011.

[17] Y. Xiao, S. Wang, L. Dan, X. Lei, P. Yang, and W. Xiang, "OFDM with interleaved subcarrier-index modulation," *IEEE Commun. Lett.*, vol. 18, no. 8, pp. 1447-1450, Aug. 2014.

[18] E. Basar, U. Aygolu, E. Panayirci, and H. V. Poor, "Space-time block coded spatial modulation," *IEEE Trans. Commun.*, vol. 59, no. 3, pp. 823-832, Mar. 2011.

[19] M. Nakao, T. Ishihara, and S. Sugiura, "Dual-mode time-domain index modulation for nyquist-criterion and faster-than-nyquist single-carrier transmissions," *IEEE Access*, vol. 5, pp. 27659-27667, Nov. 2017.

[20] X. Cai, W. Xu, S. Hong, L. Wang and L. Zhang, "General carrier index aided dual-mode differential chaos shift keying with full mapping: design and optimization," *IEEE Trans. Veh. Technol.*, vol. 70, no. 11, pp. 11665-11677, Nov. 2021.

[21] S. Gao, M. Zhang, and X. Cheng, "Precoded index modulation for multi-input multi-output OFDM," *IEEE Trans. Wireless Commun.*, vol. 17, no. 1, pp. 17-28, Jan. 2018.

[22] G. Kaddoum, Y. Nijsure, and H. Tran, "Generalized code index modulation technique for high-data-rate communication systems," *IEEE Trans. Veh. Technol.*, vol. 65, no. 9, pp. 7000-7009, Sep. 2016.

[23] J. Li, S. Dang, Y. Huang, P. Chen, X. Qi, M. Wen, and H. Arslan, "Composite multiple-mode orthogonal frequency division multiplexing with index modulation," *IEEE Trans. Wirel. Commun.*, vol. 22, no. 6, pp. 3748-3761, Jun. 2023.

[24] J. Li, S. Dang, M. Wen, Q. Li, Y. Chen, Y. Huang, and W. Shang, "Index modulation multiple access for 6G communications: principles, applications, and challenges," *IEEE Netw.*, vol. 37, no. 1, pp. 52-60, Jan./Feb. 2023.

[25] R. Y. Mesleh, H. Haas, S. Sinanovic, C. W. Ahn and S. Yun, "Spatial modulation," *IEEE Trans. Vel. Technol.*, vol. 57, no. 4. pp. 2228-2242, Jul. 2008.

[26] J. Jeganathan, A. Ghrayeb, L. Szczecinski and A. Ceron, "Space shift keying modulation for MIMO channels," *IEEE Trans. Commun.*, vol. 8, no. 9, pp. 3692-3703, Jul. 2009.

[27] X-Q Jiang, M. Wen, M. Hai, J.n Li, and S. Kim, "Secrecy-enhancing scheme for spatial modulation," *IEEE Commun. Lett.*, vol. 22, no. 3, pp. 550-553, Mar. 2018.

[28] X-Q Jiang, H. Hai, J. Hou, J. Li, and D. Wei, "Euclidean geometries based space-time block coded spatial modulation," *IEEE J. Sel. Top. Sign. Proces.*, vol. 13, no. 6, pp. 1301-1311, Oct. 2019.

[29] X. Pei, Y. Chen, M. Wen, H. Yu, E. Panayirci, and H. V. Poor, "Next-generation multiple access based on NOMA with power level modulation," *IEEE J. Sel. Areas Commun.*, vol. 40, no. 4, pp. 1072-1083, Apr. 2022.

[30] E. Basar, M. Wen, R. Mesleh, M. Di Renzo, Y. Xiao, and H. Haas, "Index modulation techniques for next-generation wireless networks," *IEEE Access*, vol. 5, pp. 16693-16746, Jul. 2017.

[31] P. Patcharamaneepakorn, S. Wu, C.-X. Wang, E.-H.-M. Aggoune, M. M. Alwakeel, X. Ge, and M. D. Renzo, "Spectral, energy, and economic efficiency of 5G multicell massive MIMO systems with generalized spatial modulation", *IEEE Trans. Veh. Technol.*, vol. 65, no. 12, pp. 9715-9731, Dec. 2016.

[32] P. Yang, Y. Xiao, M. Xiao, and S. Li, "6G wireless communications: vision and potential techniques," *IEEE Netw.*, vol. 33, no. 4, pp. 70-75, Jul. 2019.

[33] S. Fang, K. Zheng, Y. Xiao, Y. Yang, X. Zeng and M. Xiao, "Offset spatial modulation and offset space shift keying: efficient designs for single-RF MIMO systems," *IEEE Trans. on Commun.*, vol. 67, no. 8, pp. 5434-5444, Aug. 2019.

[34] L. Dan, T. Jiang, Y. Xiao, M. Xiao, and S. Fang, "Design of offset spatial modulation OFDM," *IEEE Trans. on Commun.*, vol. 69, pp. 6267-6280, Sep. 2021.

[35] Y. Hu, L. Dan, T. Jiang and Y. Xiao, "On the design of offset spatial modulation with low PAPR," in *Proc. IEEE Veh. Technol. Conf. (VTC)*, pp. 1-6, Aug. 2022.

[36] Y. Wang, W. Xiong, Y. Xiao, S. Fang ,Y. Li, and C. Zheng, "Offset spatial modulation with multiple receive antennas," *IEEE Access*, vol. 8, pp. 100542-100550, Apr. 2020.

[37] Y. Wang, W. Xiong , Y. Xiao , S. Fang , and Y. Li, "Transmit antenna selection in offset spatial modulation systems," *IEEE Commun. Lett.*, vol. 24, pp. 1572-1576, Jul. 2020.

[38] Q. Wu and R. Zhang, "Intelligent reflecting surface enhanced wireless network: joint active and passive beamforming design," in *Proc. IEEE Glob. Commun. Conf.*, Abu Dhabi, UAE, Dec. 2018.

[39] W. Saad, M. Bennis and M. Chen, "A vision of 6G wireless systems: applications, trends, technologies, and open research Pproblems," *IEEE Netw.*, vol. 34, no. 3, pp. 134-142, Oct. 2020.

[40] E. Basar, "Transmission through large intelligent surfaces: a new frontier in wireless communications," *in Proc. Eur. Conf. Netw. Commun.*, Valencia, Spain, pp. 112-117, Jun. 2019.

[41] E. Basar, "Reconfigurable intelligent surface-based index modulation: a new beyond MIMO paradigm for 6G," *IEEE Trans. Commun.*, vol. 68, no. 5, pp. 3187-3196, May 2020.

[42] Q. Li, M. Wen, and M. D. Renzo, "Single-RF MIMO: from spatial modulation to metasurface-based modulation," *IEEE Wirel. Commun.*, vol. 28, no. 4, pp. 88-95, Aug. 2021.

[43] S. Lin, B. Zheng, G. C. Alexandropoulos, M. Wen, M. D. Renzo, and F. Chen, "Reconfigurable intelligent surfaces with reflection pttern modulation: beamforming design, channel estimation, and achievable rate analysis," *IEEE T. Wirel. Commun.*, vol. 20, no. 2, pp. 741-754, Feb. 2021.

[44] S. Lin, F. Chen, M. Wen, Y. Feng, and M. D. Renzo, "Reconfigurable intelligent surface-aided quadrature reflection modulation for simultaneous passive beamforming and information transfer," *IEEE T. Wirel. Commun.*, vol. 21, no. 3, pp. 1469-1481, Mar. 2022.

[45] K. Asmoro, and S. Y. Shin, "RIS grouping based index modulation for 6G telecommunications," *IEEE Wire. Commun. Let.*, vol. 11, no. 11, pp. 2410-2414, Nov. 2022.

[46] J. Jeganathan, A. Ghrayeb, L. Szczecinski, and A. Ceron, "Space shift keying modulation for MIMO channels," *IEEE Trans. Wireless Commun.*, vol. 8, no. 7, pp. 3692-3703, Jul. 2009.

[47] R. Hunger, *Floating point operations in matrix-vector calculus*, Munich, Germany: Munich Univ. of Technology, Institute for Circuit Theory and Signal Processing, 2005.

[48] M. K. Simon and M.-S. Alouini, *Digital communication over fading channels*. John Wiley and Sons, Ltd, 2005.

[49] H. A. David, H. N. Nagaraja, *Order statistics*. John Wiley and Sons Ltd, 2003.

Guoying Zhang (Student Member, IEEE) received the B.S. degree in school of mathematics and big Data from Dezhou University, Dezhou, China. She received the M.S. degree in College of Science from Donghua University, Donghua, China. She is currently pursuing the Ph.D. degree in information and communication intelligence system with Donghua University, Shanghai, China. Her main research interests include wireless communications, index modulation, RIS and MIMO.

Shahid Mumtaz (Senior Member, IEEE) is an IET Fellow, IEEE ComSoc and ACM Distinguished Speaker, recipient of IEEE ComSoc Young Researcher Award (2020), founder and EiC of the IET Journal of Quantum Communication, Vice-Chair of the Europe/Africa RegionIEEE Com Soc Green Communications Computing Society, and Vice-Chair of IEEE Standard P1932.1: Standard for Licensed/Unlicensed Spectrum Interoperability in Wireless Mobile Networks. He is the author of 4 technical books, 12 book chapters, 300+ technical papers (200+ IEEE journals/transactions, 100+ conference proceedings), and received 2 IEEE best paper awards in the area of mobile communications. Most of his publication is in the field of wireless communication. He is serving as Scientific Expert and Evaluator for various research funding agencies. He was awarded an Alain Bensoussan Fellowship in 2012. He was the recipient of the NSFC Researcher Fund for Young Scientist in 2017 from China.

Xue-qin Jiang (Senior Member, IEEE) received the B.E. degree in computer science from the Nanjing Institute of Technology, Nanjing, China, and the M.S. and Ph.D. degrees in electronics engineering from Chonbuk National University, Jeonju, South Korea. He is currently a Professor with the College of Information Science and Technology, Donghua University, China. He has authored or coauthored more than 80 journal articles. His research interests include wireless communications, quantum key distribution, signal processing, and machine vision. He is also serving as an AE for IEEE Communications Letters and IEEE Access.

Han Hai (Member, IEEE) received his B.S. degree in information and computing sciences from South Central University for Nationalities, P.R. China, and the M.S. and the Ph.D. degrees in electronics engineering from Chonbuk National University, Korea, in 2013 and 2018, respectively. He is currently an assistant professor at College of Information Science and Technology, Donghua University, Shanghai, China. His research interests include wireless communications, MIMO and spatial modulation.

Lexi Xu (Senior Member, IEEE) received M.S. and PhD degrees from Beijing University of Posts and Telecommunications, Beijing, China, and Queen Mary University of London, London, United Kingdom, in 2009 and 2013, respectively. From 2013 to 2020, he was a senior engineer at Network Technology Research Institute, China United Network Communications Corporation (China Unicom). Since late 2020, Dr. Xu is now a professor level senior engineer at Research Institute, China Unicom. He is also a China Unicom delegate in ITU, ETSI, 3GPP, CCSA. He also serves as a professor (part-time) at Beijing University of Posts and Telecommunications. His research interests include big data, self-organizing networks, satellite system, radio resource management in wireless system, etc.